First-Principles Calculations and Microscopic Mechanism Study of Superconducting Vortex Pinning

Haozhe Shi, Yuncheng Xie, Weibin Chu, Xin-Gao Gong

Department of Physics; State Key Laboratory of Surface Physics; Key Laboratory of Computational Physical Sciences (MOE);
Fudan University, Shanghai 200433, China

Point Defects Pinning

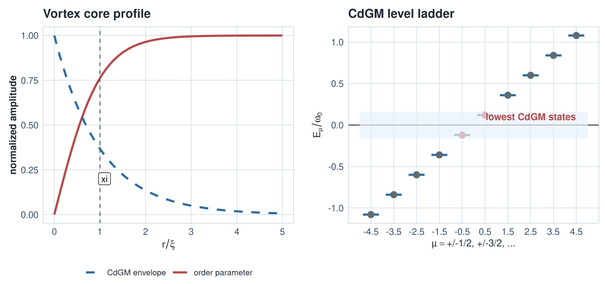

Figure. Point defects can pin vortices not only by reducing condensation-energy cost, but also by reshaping CdGM-like low-energy vortex-core states.

- In the superconducting state, a point defect in FeSe/FeTe acts as a pinning center that attracts a vortex core upon alignment.
- Compare Fe-site vacancies, chalcogen-site vacancies, and Fe→Cu substitution in one protocol.
- Compute U_{pin}, f_{p}, and the quasiparticle/condensation decomposition.

VASP–Wannier–BdG Workflow

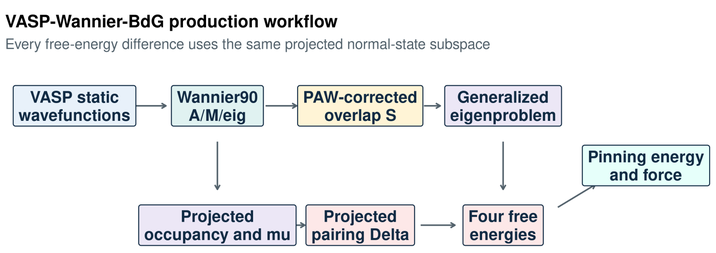

Figure. Production route from VASP static wave functions to native Wannier90 export, PAW-corrected overlap, projected occupancy, projected BdG, and finally U_{pin}, f_{p}.

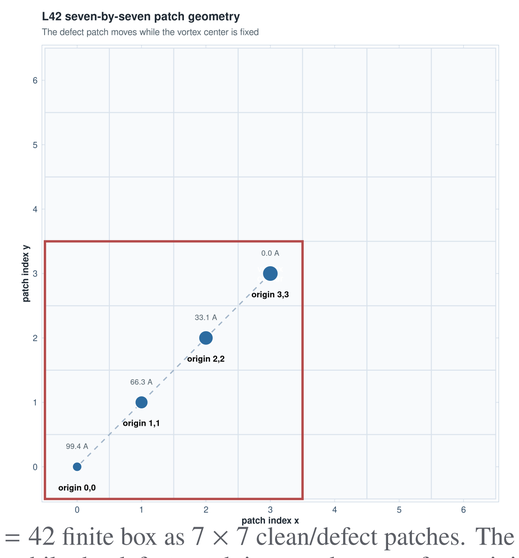

Figure. $L = 42$ finite box as 7×7 clean/defect patches. The vortex center is fixed, while the defect patch is moved among four origins.

- Clean and defect Wannier bases are gauge-aligned before stitching H_0 and S.
- VASP normal-state information is compressed into a patch-resolved low-energy Hamiltonian.

Four-Patch Energy

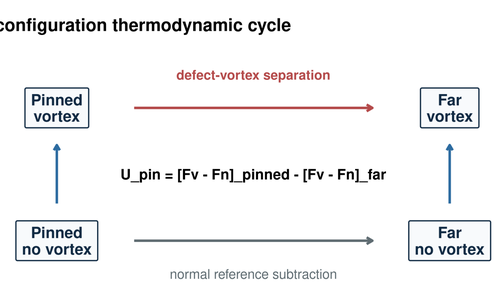

Figure. The vortex/no-vortex subtraction is performed at the same defect origin before comparing the pinned and far-reference geometries.

$$U_{\mathrm{pin}} = \left[F_v - F_n\right]_{(3,3)} - \left[F_v - F_n\right]_{(1,1)}$$

- $(3,3)$ is the defect-vortex coincident configuration; $(1,1)$ is the buffered far reference.
- The subtraction removes defect-only static contributions before the pinned/far comparison.
- Negative U_{pin} means that inserting a vortex costs less free energy when the vortex sits on the defect.

Low-Energy Subspace

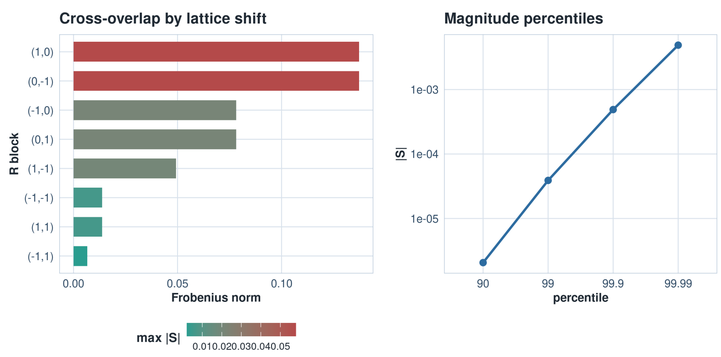

Figure. The stitched clean–defect basis is localized but not orthonormal; the PAW-corrected overlap matrix S is retained explicitly.

$$H_0 C = SCE, \qquad C^\dagger S C = I$$

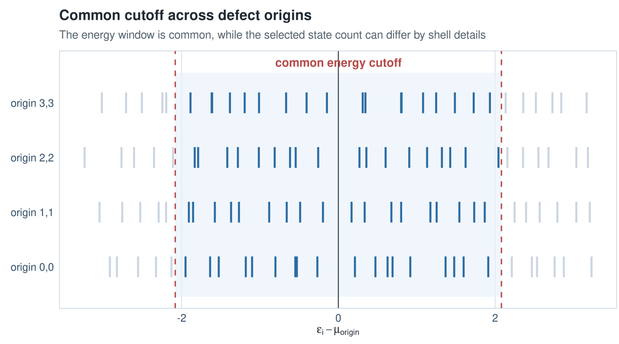

Figure. Different defect origins have slightly different shell structures. A common energy cutoff compares the same physical low-energy window.

- μ is fixed by projected occupancy of the Wannier subspace.
- Ω_{qp}, E_{cond}, $g(E_c)$, and cutoff selection share one projected subspace.

Main Results

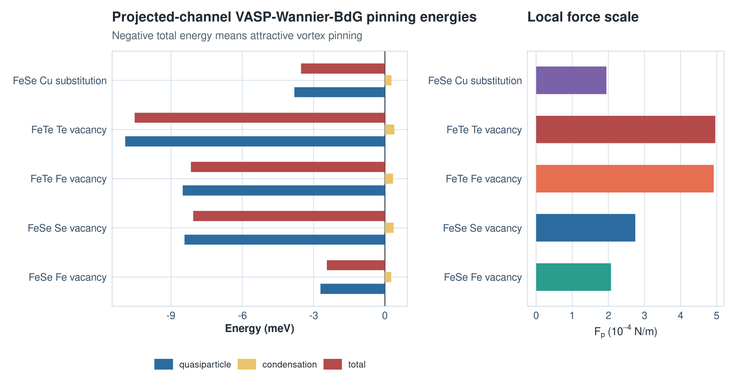

Figure. Pinning-energy decomposition and $(3,3) \rightarrow (2,2)$ local unit-length forces for the five production systems.

System	U_{pin} (meV)	$U_{\mathrm{pin}}^{\mathrm{qp}}$	f_{p} (N/m)
FeSe Fe vacancy	-2.4457	-2.7133	2.08×10^{-4}
FeSe Se vacancy	-8.0610	-8.4267	2.75×10^{-4}
FeTe Fe vacancy	-8.1633	-8.5002	4.92×10^{-4}
FeTe Te vacancy	-10.5291	-10.9194	4.96×10^{-4}
FeSe Cu substitution	-3.5251	-3.8059	1.95×10^{-4}

FeSe Fe vacancy vs. experiment

Reference	Extraction	f_{p} (N/m)
Transport exp.	low-field $F_p = J_c B$, $f_{\mathrm{p}} = J_c \Phi_0$	0.8×10^{-4}
STM exp.	$-\partial U_{\mathrm{pin}}/\partial d$ near dumbbell defect	2.4×10^{-4}
This work	FeSe Fe vacancy BdG free-energy slope	2.08×10^{-4}

Distance-Resolved Pinning

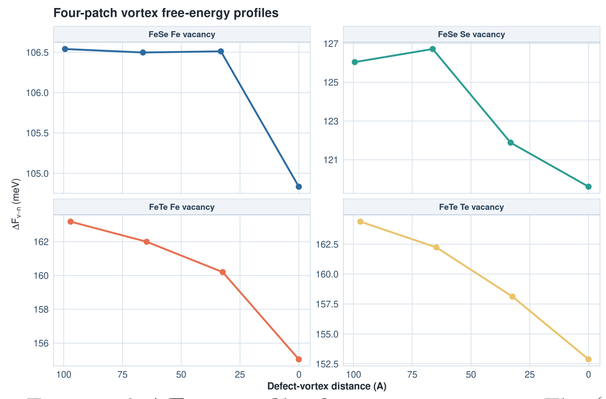

Figure. Four-patch ΔF_{v-n} profiles for vacancy systems. The $(3,3)$, $(2,2)$, $(1,1)$, and $(0,0)$ origins form a discrete pinning-potential profile.

Microscopic Mechanism

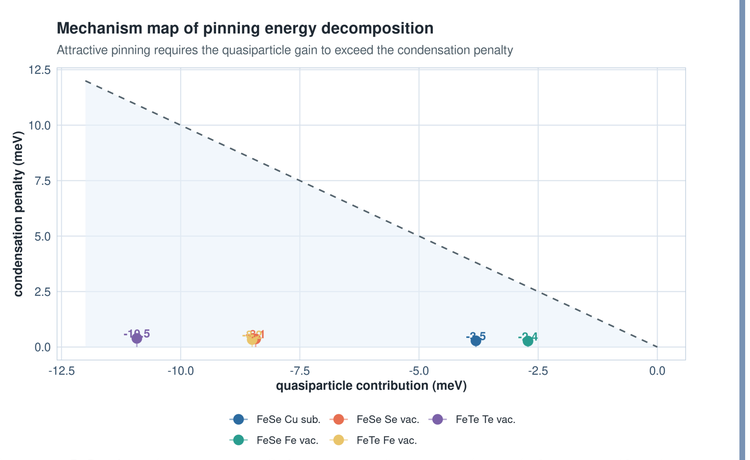

Figure. Mechanism map of the attractive quasiparticle contribution versus the projected-channel condensation penalty. All production systems lie in the attractive region.

- $U_{\mathrm{pin}}^{\mathrm{qp}} < 0$: defect-vortex coincidence lowers the vortex-core quasiparticle spectral cost.
- $U_{\mathrm{pin}}^{\mathrm{cond}} > 0$: local pairing-energy loss partially compensates the attraction.
- The final ranking is controlled by defect scattering, CdGM-state reconstruction, and pairing-energy loss, not by order-parameter suppression alone.

HamNet–OpenMX Route

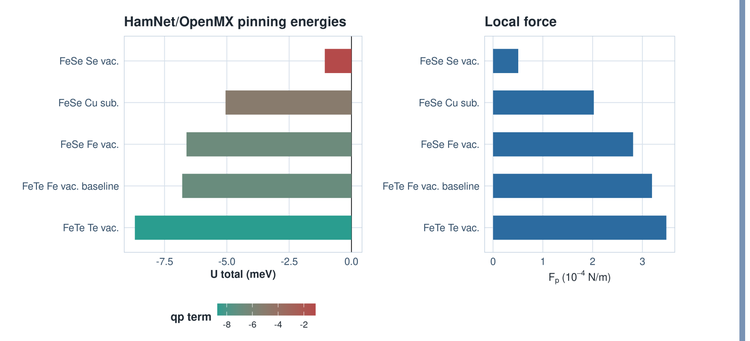

Figure. HamNet/OpenMX active-AO route gives attractive far-reference pinning for the tested systems and provides a fast trend-screening branch.

$$\text{structure} \rightarrow H_{\mathrm{AO}}/S_{\mathrm{AO}} \rightarrow \text{generalized spectrum} \rightarrow (U_{\mathrm{pin}}, f_{\mathrm{p}})$$

- Replaces the expensive VASP–Wannier normal-state generator with an active-AO Hamiltonian route.
- Keeps the same vortex/no-vortex and pinned/far free-energy definitions as the main workflow.
- Current role: fast trend prescreening; meV-level use still needs OpenMX benchmarks, energy-zero calibration, active-space checks, and cutoff audits.

Robustness and Extension

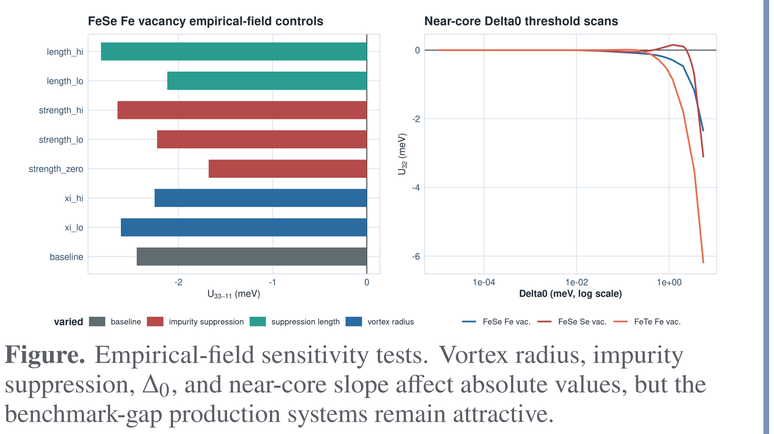

Figure. Empirical-field sensitivity tests. Vortex radius, impurity suppression, Δ_0, and near-core slope affect absolute values, but the benchmark-gap production systems remain attractive.

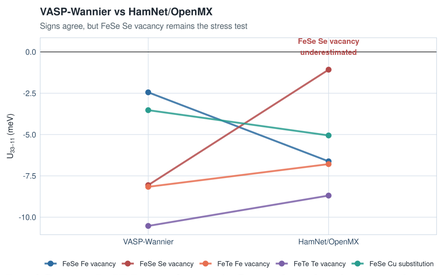

Figure. HamNet/OpenMX active-AO calculations close a structure-to-BdG loop and can support trend prescreening, but still underestimate some meV-scale free-energy differences.

- FeTe vacancies remain attractive for $\Delta_0 = 3.3, 4.5, 5.5$ meV.
- HamNet/OpenMX, FeS, self-consistent pairing, Peierls magnetic fields, HSE, and YBCO tests define the next extension boundaries.